Proceedings of the ASME 2019
International Design Engineering Technical Conferences
and Computers and Information in Engineering Conference
IDETC/CIE2019
August 18-21, 2019, Anaheim, CA, USA

DETC2019-97119

SIMULATING COMPLIANT CREASE ORIGAMI WITH A BAR AND HINGE MODEL

Yi ZHU
Department of Civil and Environmental Engineering
University of Michigan
Ann Arbor, Michigan 48109
Email: yizhucee@umich.edu

Evgueni T. Filipov*
Department of Civil and Environmental Engineering
University of Michigan
Ann Arbor, Michigan 48109
Email: filipov@umich.edu

ABSTRACT

Small-scale origami inspired assemblages are usually made with soft compliant plates to serve as creases because it is difficult to fabricate real hinges at those scales. In most conventional origami modeling techniques, these soft and compliant creases are usually neglected and simplified as concentrated rotational springs. Such simplification does not capture the three dimensional geometry correctly and also neglects torsional and extensional deformations of the compliant creases. These deformations could be significant for determining advanced mechanical behaviors of the origami such as bistablity and multistablity. In this paper an improved formulation of a simple bar and hinge model is proposed to capture the geometry and flexibility of compliant creases. Equations for assigning bar areas and spring stiffness are derived based on the theoretical plane stress plate models and the pseudo-rigid model. These equations are next verified against finite element simulations for both infinitesimal stiffness and large deformation stiffness. It is found that the proposed model can predict stiffness characteristics of compliant crease origami relatively well. Furthermore, two examples are used to demonstrate the efficiency and capability of the proposed model.

INTRODUCTION

Origami inspired assemblages provide a feasible and convenient approach for designing reconfigurable structures and metamaterials with special mechanical properties. Various engineering structures of this type have been proposed in the past decades, such as reconfigurable facades and canopies [1], bistable wings [2], mechanical memory devices [3], pneumatic actuators [4] and various meta-materials [5, 6].

In order to understand the mechanical and kinematic properties of origami assemblages, realistic simulation models are needed. Although finite element (FE) simulations tend to provide a possible solution, the extended model building and long computation time make them difficult to use at a preliminary design stage, where instant feedback is desired. Several simplified models have been proposed to simulate the behavior of origami structures [7–10], and among them, two of the most widely used are rigid folding models and bar and hinge models.

The rigid folding models assume rigid panels and concentrate all deformation within creases. Numerical codes of this type are based on rigid folding constraints imposed by crease patterns. For example, one widely used necessary condition for rigid folding is that the rigid body rotations about a vertex sum to unity as $R_1R_2...R_n = I$, where R_i are the the rotation matrices and I is identity [11]. The detailed equations for expressing R_i can be found in [12]. Widely used numerical simulations of this type include Tachi's rigid origami simulation code for triangulated general patterns [7] and quad origami patterns [8].

The bar and hinge models simulate an origami pattern using extensional bar elements and rotational springs so that they can further capture the deformation of panels. Models of this type have been used to study small strain behaviors [13] as well as large strain behaviors of origami tessellations [9, 10]. Moreover, they were also used in analyzing the mechanical characteristics

*Address all correspondence to this author.

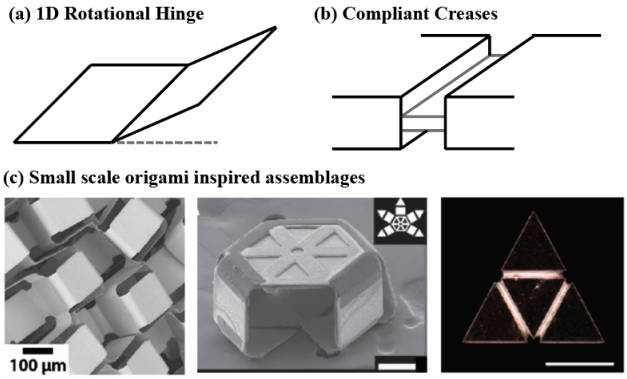

FIGURE 1. (a) Simplification of a crease in common origami simulation models; (b) Thick panels with a distributed hinge region; (c) Small-scale origami inspired structures typically have a distributed compliant crease region. Figures from left to right are from [16–18].

of origami inspired metamaterials [1, 14]. A number of different variations of bar and hinge models were developed and studied in detail [9, 15].

These two common origami simulation methods simplify creases as concentrated 1D rotational springs that have infinitesimal width (Fig. 1 (a)). However, in small-scale applications, it is difficult to fabricate discrete hinges (such as those on our doors) and actuate them, so small-scale origami are usually composed of softer compliant creases and stiffer panels (Fig. 1 (b) and (c)). In those applications, the existence of compliant creases introduces additional degrees of freedom and allows the structure to achieve richer deformations.

The "smooth fold" model developed by Hernandez and his coauthors [19, 20] was one of the first to explicitly simulate the behavior of compliant creases without a FE discretization. This model is based on the rigid panel assumption and solves the deformed configuration by considering the geometric constrain imposed by the crease pattern. This model is capable of capturing accurate local geometry of compliant creases, including the curvature and relative extension, and saves 30% of computation times when compared with FE simulations [19]. The model was used for designing a reconfigurable antenna [21] and a solar powered underwater vehicle [22]. Although this model is a state-of-the-art in the modeling of compliant creases in origami assemblages, and can capture the exact folded geometry, its derivation is complicated and it requires long computation time. Another limitation of the model is that it cannot capture the flexibility of panels, because it uses a rigid panel assumption.

In this article, a relatively simple and computationally efficient bar and hinge model for compliant crease origami is developed and tested. By including additional bars and rotational springs in the crease area, the model is capable of capturing the additional torsional and extensional deformation in these compliant creases. The model provides a computationally efficient solution for solving a large number of compliant crease origami structures within a short period of time at a preliminary design stage. This paper first presents the formulation of the proposed compliant crease bar and hinge model, which is based on fundamental plate theories and the pseudo-rigid model. Next, a thorough verification is performed to compare the accuracy of the proposed model against FE simulations. Finally, two examples are used to demonstrate the efficiency and capability of the model.

DERIVATION OF MODEL STIFFNESS PARAMETERS

Compliant crease modeling

In bar and hinge models, the *bar* refers to the extensional element that provides in-plane stiffness for shearing and stretching. The *rotational spring* (hinge) refers to the rotational element about a bar axis that provides out-of-plane stiffness for crease bending and panel bending. We refer to references such as [9, 10] for details on how these elements are computationally formulated, but focus on their stiffness definitions in this article. In this paper, the *crease* is different from the rotational spring and it refers to the shaded area shown in Fig. 2 (a), which is a collection of several bars, rotational springs, and nodes.

The proposed meshing technique is based on the observed natural behavior of an origami assemblage with compliant creases. When a compliant crease is folded, the curvature of the crease is evenly distributed across the width (Fig. 2 (b)). The proposed model captures this more even distribution of the curvature and the three-dimensional geometry by using three lines of rotational springs instead of just one. Two rotational springs connect the panels to the crease area, and two half-length rotational springs are located along the center of the crease region. When relative torsion occurs between two panels, the connecting crease deforms diagonally, as indicated in the Fig. 2 (c). This behavior is captured with the four additional rotational springs placed diagonally within the crease region. Notably, this meshing technique also captures the extensional stiffness of creases, which can play a significant role in analyzing bistable and multistable behaviors of origami [2].

Derivation of bar areas

The compliant crease bar and hinge model can be defined based on the following geometric parameters: the crease width W, crease length L, crease thickness t_{crease}, and panel thickness t_{panel} (Fig. 3 (a)). Bar areas of the model are determined by matching the stiffness of the bar and hinge model with a theoretical plate model of the same bulk material. The bars within a crease region are divided into four different groups as shown

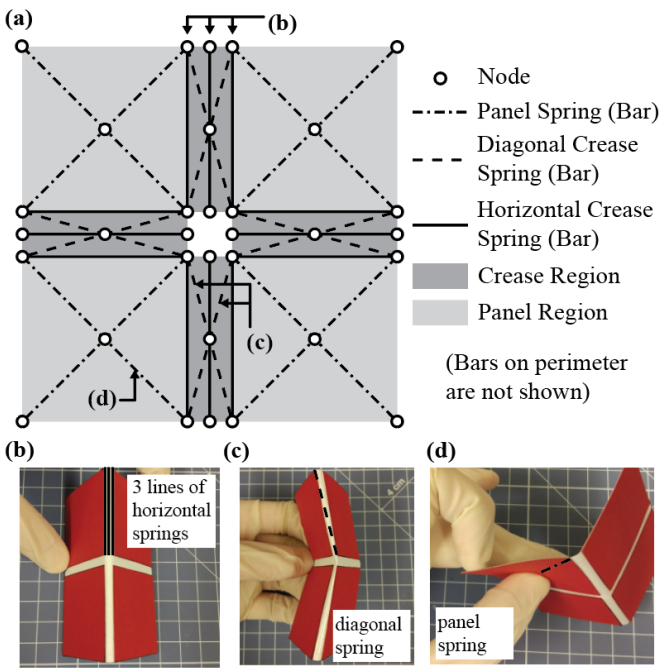

FIGURE 2. (a) Bar and hinge representations used in this paper; (b) Three lines of horizontal springs are used to better mimic the evenly distributed curvature in compliant creases; (c) Diagonal springs are used to capture relative torsion between panels; (d) Panel springs are used to mimic the behavior of panel bending.

in the Fig. 3 (b). The area of A_0 bars is later determined in the panel modeling section and is temporarily assumed to be infinite in this section. This assumption generally works well because panels are usually much thicker and thus stiffer than creases.

The area of A_1 bars is calculated such that they produce the same stiffness as a plane-stress plate under a uniform tensile loading (Fig. 3(c)). The stiffness of the plate is calculated by applying a unit normal strain field $\vec{\varepsilon} = [1\ 0\ 0]^T$ and the total extensional stiffness of the plate model is obtained as:

$$k_{a,pl} = \frac{\frac{E_{crease}}{1-\nu_{crease}^2} t_{crease} L}{W}, \tag{1}$$

where the E_{crease} and ν_{crease} are the Young's modulus and Poisson's ratio of the crease region respectively. The axial stiffness of the compliant crease in the bar and hinge model is calculated with one additional assumption: the contribution of diagonal bars (A_2 bars) is neglected because of their large inclination. This assumption tends to be valid because the crease length L is typically much larger than its width W. With this additional assumption, only four A_1 bars are contributing to the axial stiffness and thus

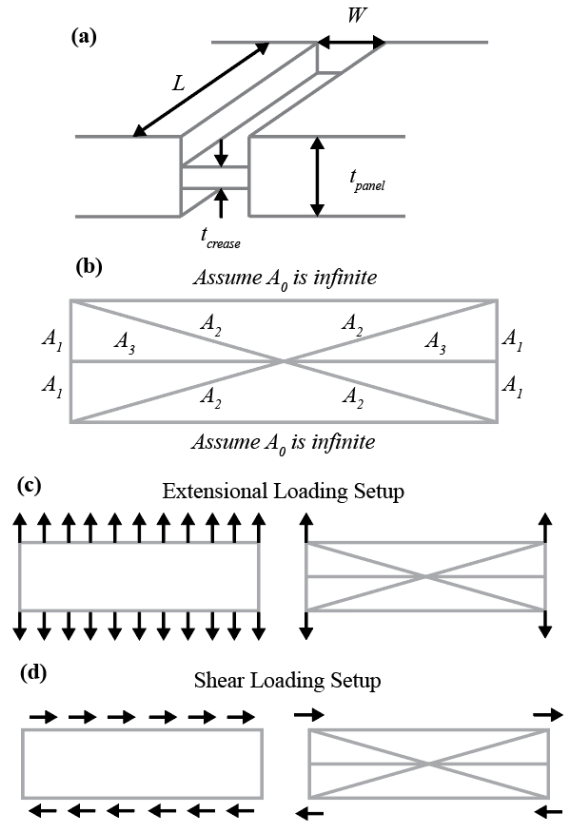

FIGURE 3. (a) Definition of geometric parameters used in the stiffness derivation; (b) Bar areas within the compliant crease region; (c) Illustration of axial loading used to determine A_1 bar areas; (d) Illustration of shear loading used to determine A_2 bar areas.

the stiffness of the bar and hinge model is calculated as:

$$k_{a,BH} = \frac{2EA_1}{W}. \tag{2}$$

By setting $k_{a,BH} = k_{a,pl}$, we solve the assigned area for A_1 bars as:

$$A_1 = \frac{Lt_{crease}}{2(1-\nu_{crease}^2)}. \tag{3}$$

Similarly, the area of diagonal bars (A_2 bars) is set such that they produce the same shear stiffness as a plate with the same bulk material. A unit shear strain field $\vec{\varepsilon} = [0\ 0\ 1]^T$ is applied and the shear stiffness of the plate is calculated as:

$$k_{s,pl} = \frac{E_{crease} t_{crease} L}{2W(1+\nu_{crease})}. \quad (4)$$

Because A_0 bars are assumed to have infinite area, only the diagonal bars are contributing to the shear deformation in the bar and hinge model. Therefore, the shear stiffness of the bar and hinge model can be calculated as:

$$k_{s,BH} = \frac{2E_{crease} A_2}{(W^2+L^2)^{1.5}} L^2. \quad (5)$$

Similarly, by setting $k_{s,BH} = k_{s,pl}$, we can solve the assigned areas for A_2 bars. It is further assumed that A_3 bars have the same area as the A_2 bars. Overall, the A_3 bars do not contribute significantly either to tensile or shear behaviors, because they are orthogonal to the edge of the crease region. Although this asumption is somewhat crude, it greatly simplifies the formulation and gives results that match FE simulations relatively well as will be demonstrated in following sections. The areas of A_2 and A_3 bars are thus calculated as:

$$A_3 = A_2 = \frac{(L^2+W^2)^{1.5}}{4(1+\nu_{crease})} \frac{t_{crease}}{LW}. \quad (6)$$

Derivation of rotational spring stiffness

In this article, upper case K_{spr} denotes the length-normalized spring stiffness, and the lower case k_{spr} is the total stiffness of the rotational spring, which is calculated as:

$$k_{spr} = K_{spr} L_{spr}, \quad (7)$$

where L_{spr} is the length of the rotational spring. A compliant crease within an origami structure can be treated as a compliant mechanism and modeled as a single rotational spring using the pseudo-rigid model described in [23] (Fig. 4 (b)). The rotational stiffness of the corresponding pseudo-rigid crease model is given as:

$$k_{crease} = \frac{E_{crease} I}{W} = \frac{E_{crease} L t_{crease}^3}{12W}. \quad (8)$$

In the proposed model, this single rotational spring is further divided into three lines of springs (The four K_{spr1} in Fig. 4 (a) and (b)) to better match the distributed curvature observed in real compliant creases. Because one spring is split into three lines of springs, the rotational stiffness of each spring should be increased by a factor of three such that it produces the same global stiffness as the one-spring pseudo-rigid model. Thus the normalized rotational spring stiffness for these four K_{spr1} springs is given as:

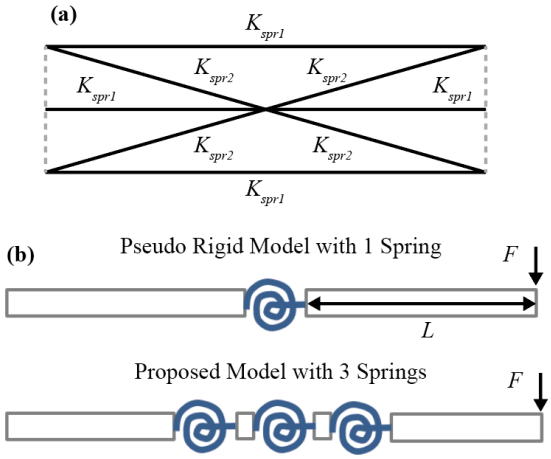

FIGURE 4. (a) Rotational spring stiffness components used in the compliant crease region; (b) Comparison of the one-spring pseudo-rigid model and the proposed three-spring compliant crease bar and hinge model.

$$K_{spr1}^{BH} = \frac{3E_{crease} I}{WL} = \frac{E_{crease} t_{crease}^3}{4W}. \quad (9)$$

It is difficult to solve the stiffness of the four diagonal rotational springs K_{spr2} using previous strategies and thus their stiffness is obtained by matching the results from FE simulations of compliant creases. A factor f is used to scale the stiffness of K_{spr2} with respect to K_{spr1} as shown in Eqn. 10. A factor of $f = 4$ best matches the FE results and thus in the following sections, K_{spr2} is calculated as:

$$K_{spr2} = f K_{spr1} = 4K_{spr1} = \frac{4 \times 3E_{crease} I}{WL} = \frac{E_{crease} t_{crease}^3}{W}. \quad (10)$$

It makes sense that this factor f should be greater than one, because the corresponding diagonal deformations have more concentrated curvatures as shown on Fig. 2 (c), and thus the diagonal springs should be stiffer. Details on the performance of this assigned $f = 4$ will be demonstrated in the following verification section.

Modeling of panels

The area of the bars within panels is calculated using the generalized N5B8 model derived in [15] as shown in Eqn. (11). The equation is formulated with the panel area S and total length of the bars L_i within the panel, and is derived such that the strain energy is preserved when the panel undergoes uniform in-plane dilation.

$$A_{panel} = \frac{2St_{panel}}{(1-\nu)\sum_{i=1} L_i} \tag{11}$$

The rotational spring stiffness within the panel is derived based on the knowledge that bending stiffness scales with the cubic of thickness and the material stiffness [24]. The cubic of the ratio between panel thickness and crease thickness and the ratio of Young's modulus are used to scale the normalized crease stiffness to obtain the stiffness for panel springs as:

$$K_{panel} = \frac{E_{panel}t_{panel}^3}{E_{crease}t_{crease}^3}K_{crease} = \frac{E_{panel}t_{panel}^3}{4W}. \tag{12}$$

More robust models for bar and hinge formulations of origami panels as those in [9] could be used, but they are derived based on fully restrained panel edges. For the purpose of this article, these two simple equations work relatively well because the deformation of panels is usually not the controlling factor that governs the global behavior of compliant crease origami as will be shown in the example section.

MODEL VERIFICATION

In this section, the proposed compliant crease bar and hinge model is compared against FE simulations to improve its performance, and explore its accuracy. This verification is divided into two parts: infinitesimal stiffness and large deformation stiffness. Two indexes, *Crease Aspect Ratio* and *Thickness Ratio*, are defined to quantify the geometrical characteristics of compliant creases. *Crease Aspect Ratio* is defined as: $\alpha = W/L$, where W and L are crease width and crease length respectively (see Fig. 3 (a)). The *Thickness Ratio* is defined as: $\beta = t_{panel}/t_{crease}$, where t_{panel} and t_{crease} are the thickness of panels and creases respectively. These two indexes describe geometric properties of compliant crease origami that affect the local and global stiffness of the system. Common origami designs with compliant creases typically have a Crease Aspect Ratio $\alpha \approx 0.1$ and a Thickness Ratio $\beta \approx 3.0$ [16, 18]. In the following verification sections, the elastic moduli of creases and panels are set to be $E_{crease} = E_{panel} = 2$ GPa, while the Poisson's ratios of both creases and panels are set as $\nu_{crease} = \nu_{panel} = 0.3$, which are realistic values of soft crease origami assemblages.

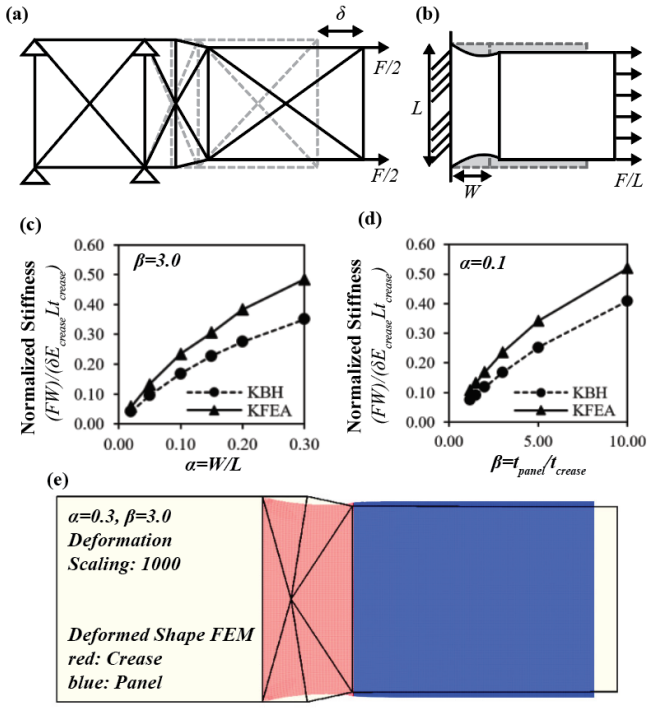

FIGURE 5. Infinitesimal tensile stiffness verifications. (a) Tensile loading of the proposed bar and hinge model; (b) Tensile loading of the FE model used for verification; (c) Comparison of the tensile stiffness prediction with respect to α; (d) Comparison of the tensile stiffness prediction with respect to β; (e) Comparison of the deformed shapes of the proposed bar and hinge model and the FE simulation.

Infinitesimal stiffness verification

Four types of loading are checked in the infinitesimal stiffness verification. They are tensile, shear, bending and torsional loading. Stiffness predictions from the compliant crease bar and hinge model are compared against FE simulations when varying α values or β values. The value of α is changed by varying W while fixing $L = 2.0$cm, and the value of β is changed by varying t_{panel} while fixing $t_{crease} = 0.1$ mm. These values were selected because they represent realistic small-scale origami structures.

The tensile verification for the bar and hinge model with respect to the FE simulation is shown in Fig. 5. Infinitesimal stiffness of both models is normalized by $E_{crease}Lt_{crease}/W$ to give a dimensionless result. The proposed bar and hinge model is about $10-25\%$ softer than the FE simulation for all explored geometric variations of the structure. This difference is attributed to the error in the panel region rather than the crease region as demonstrated in the Fig. 5 (e). The generalized N5B8 panel model as defined in Eqn. (11) does not capture the Poisson's effect correctly and underestimates the stiffness because it only matches

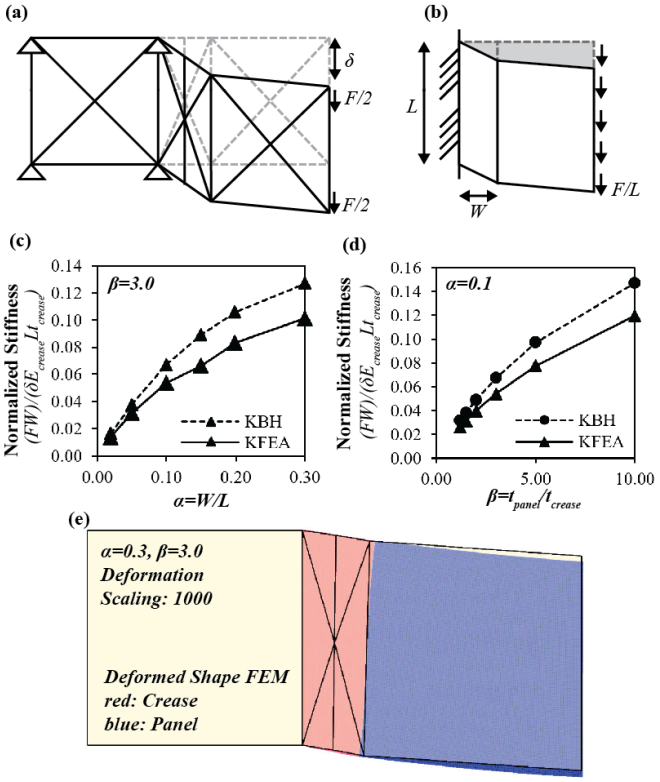

FIGURE 6. Infinitesimal shear stiffness verifications. (a) Shear loading of the proposed bar and hinge model; (b) Shear loading of the FE model; (c) Comparison of the shear stiffness prediction with respect to α; (d) Comparison of the shear stiffness prediction with respect to β; (e) Comparison of deformed shapes of the proposed bar and hinge model and the FE simulation.

the strain energy under uniform dilation. The total amount of deformation δ in the compliant crease region appears appropriate, however the deformed shape does not match the FE simulation exactly.

The results of shear verification are summarized in Fig. 6. Similar to the tension case, the stiffness plotted is normalized by $E_{crease}Lt_{crease}/W$ to give dimensionless results. Figure 6 (c) and (d) show that the mismatch between the bar and hinge model and FE simulation is around $10-15\%$, with the bar and hinge model predicting stiffer responses. This difference is primarily due to the error in the model formulation of panels rather than of creases (see Fig. 6 (e)) due to the same reason discussed in the tensile verification.

Figure 7 (a) and (b) illustrate the loading set up for infinitesimal bending verification and the results are plotted in Fig. 7 (c) and (d). The stiffness predictions from the two models match well for different α values when $\beta \approx 3.0$ as illustrated in Fig. 7

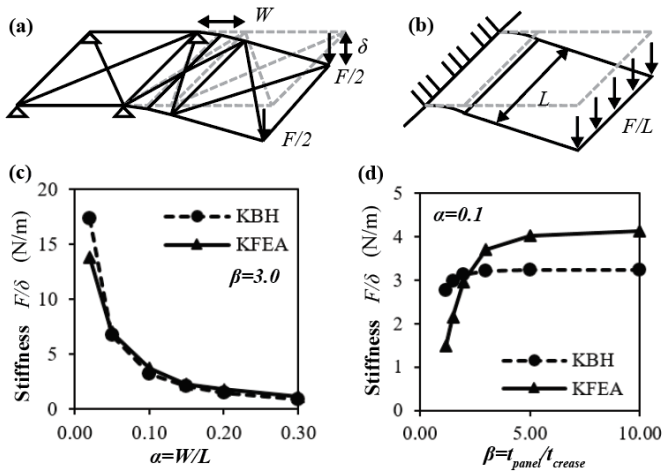

FIGURE 7. Infinitesimal bending stiffness verifications. (a) Bending loading of the proposed bar and hinge model; (b) Bending loading of the FE model; (c) Comparison of the bending stiffness prediction with respect to α; (d) Comparison of the bending stiffness prediction with respect to β.

(c). When β becomes large ($\beta > 5$), the stiffness mismatch between the two models reaches an asymptotic value of about 25%. This mismatch is due to the additional diagonal rotational springs K_{spr2} that are introduced to capture torsional deformations of the crease. These diagonal springs soften the bending stiffness of the crease by introducing additional degrees of freedom. The softening is much less aparent at larger strains, as will be demonstrated in the following section. When β is small, the mismatch is larger because bending of panels is significant in the global deformation and it is not captured by the bar and hinge model.

The verification of torsional stiffness is summarized in Fig. 8. The results only match well when $\alpha \approx 0.1$ and differ significantly otherwise. When α is small, the contribution of torsional deformation from the panel is large, while when α is large the pseudo rigid model proposed in Eqn. (8) does not hold. The bar and hinge model is not well suited for capturing these torsional deformations over a wide range of α values, and thus, we tune the factor f in Eqn. (10) such that realistic results are obtained for a typical compliant crease region with $\alpha \approx 0.1$. The torsion results match well for different values of β when $\alpha = 0.1$ as shown in Fig. 8 (d).

Overall, the proposed bar and hinge model can predict infinitesimal stiffness of origami assemblages relatively well. The proposed model matches FE simulation well when $\alpha \approx 0.1$ and $\beta \approx 3.0$, which are typical values found in real origami inspired engineering structures. Exceeding these ranges tends to create errors in the simulations, but these errors are often still within acceptable ranges. Considering that the proposed compliant crease

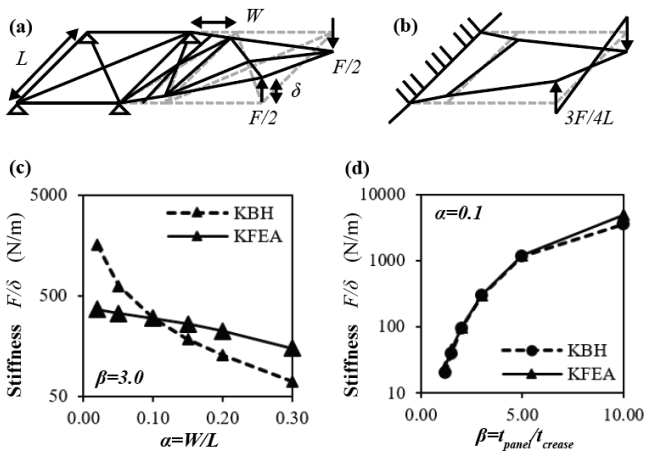

FIGURE 8. Infinitesimal torsional stiffness verifications. (a) Torsion loading of the proposed bar and hinge model; (b) Torsion loading of the FE model; (c) Comparison of the torsion stiffness prediction with respect to α; (d) Comparison of torsion stiffness prediction with respect to β.

bar and hinge model only has about one tenth of the degrees of freedom when compared with a coarsely meshed FE simulation, this accuracy is acceptable.

Large Deformation Stiffness Verification

In the verification of large deformation stiffness, only pure bending and combined bending and torsion are studied because shear and tensile deformations are substantially smaller. Two methods are used to compare compliant crease bar and hinge model with the FE simulation: (1) *Relative error* is used to measure the influence of β on the difference in response between the two models because force displacement curves generally overlaps for different values of β; (2) Force displacement curves are used to demonstrate the influence of the α value, because relative error did not show clear correlation as α changes. The relative error is defined as:

$$Error = \frac{1}{N}\sum_{i=1}^{N}\frac{\sqrt{(\delta_i^{FEA}-\delta_i^{BH})^2}}{\delta_i^{FEA}}, \tag{13}$$

where N is the total number of load increments, and δ_i^* is the predicted deformation of the i^{th} load increment from the different models. The loading was set-up such that the two models have the same force increment sequence. In the following verifications, α is varied by fixing $L = 2.0$ cm while changing W, and β is varied by fixing $t_{crease} = 0.1$ mm while changing t_{panel}.

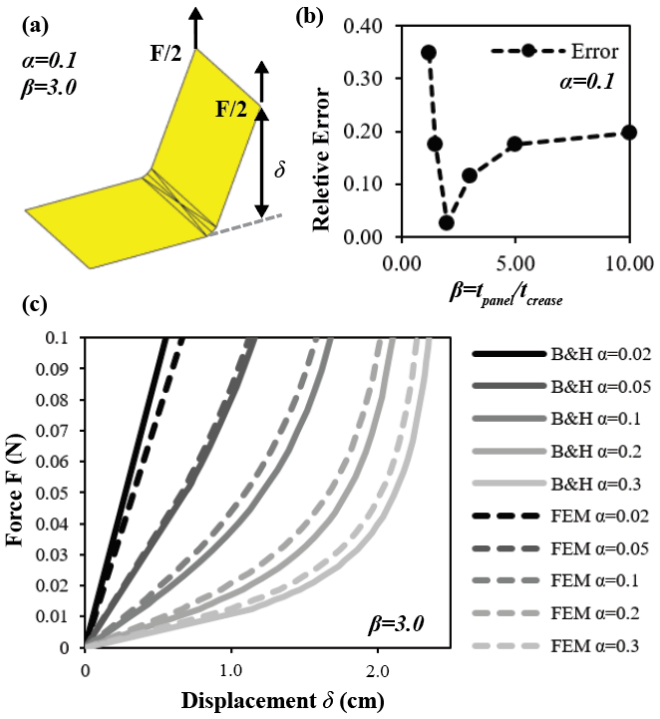

FIGURE 9. Comparison for large deformation bending. (a) Loading and deformation of the bar and hinge model ($\alpha = 0.1, \beta = 3.0$); (b) Change in relative error as the β value changes; (c) Force displacement curves when the α value changes.

Figure 9 (a) illustrates the loading set up for verification of large deformation bending. Figure 9 (b) shows that the bar and hinge model matches the FE model well when β is around 2 to 3. The error reaches an asymptotic value of 20% as β becomes large. This mismatch is also due to the additional diagonal springs K_{spr2}, which add additional flexibility as described in the infinitesimal bending section. When $\beta < 1.2$, the results from the bar and hinge model become highly offset from the FE model. This offset is because the proposed bar and hinge model is not able to capture the bending behavior of the relatively thin panels. The large error when $\beta < 1.2$ is not of a concern because realistic origami inspired structures with compliant creases usually have a larger β. Our verification indicates that the relative error is less affected by the α index and is around 5% to 10% for all α tested. Thus, the force displacement curves are plotted to better illustrate the influence of the α value. Figure 9 (c) shows that the compliant crease bar and hinge model matches the FE simulation relatively well for all α values tested when $\beta = 3.0$.

Figure 10 shows the results for the verification of combined torsional and bending loading case. The trends found in the combined torsion and bending case are similar to those found in the pure bending case with large strain. When $\beta > 2.0$, the relative

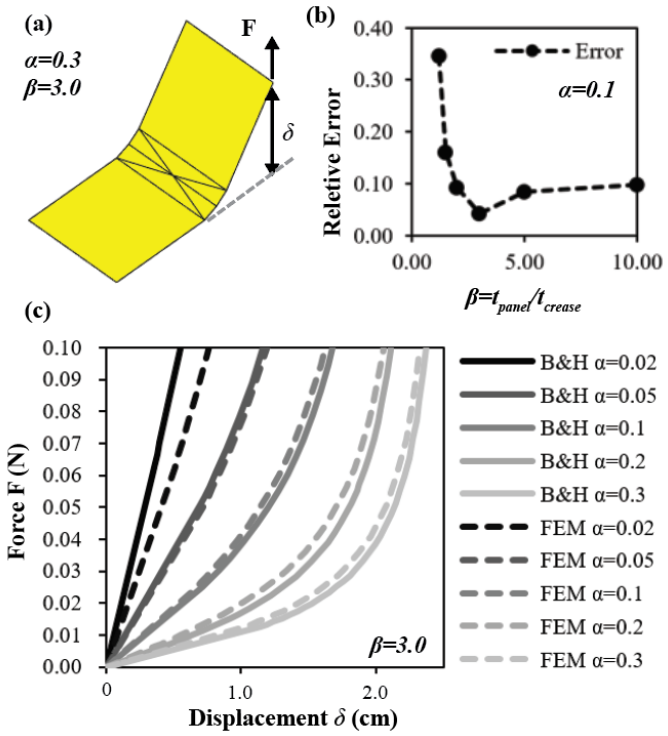

FIGURE 10. Comparison for large deformation under combined bending and torsion. (a) Loading and deformation of the bar and hinge model ($\alpha = 0.3, \beta = 3.0$); (b) Force displacement curves when the α value changes.

error between the FE simulation and the proposed bar and hinge model varies between 5% to 10%. Larger errors are observed as the panels become very thin ($\beta < 1.2$). Similarly, the force displacement curves are plotted for various α values and the relative errors for these curves are between 5% to 10%.

SIMULATION EXAMPLE

Folding of A 4-Vertex Pattern

To demonstrate the capability and efficiency of the proposed model, we simulate the folding of a 4-vertex pattern by applying external loads as demonstrated in [19]. The loading is set up according to the same model in [19] and the equilibrium is traced with a modified general displacement controlled method used in [10]. Because the detailed dimensions of structure were not provided in the reference, the dimensions used in the bar and hinge model are assumed such that they provide a similar shape. The thickness of panels is assumed to be five times the thickness of creases, so that the structure behaves like a rigid panel origami. Although the bar and hinge model cannot recreate the exact smooth curvature at the folds, it provides the same global

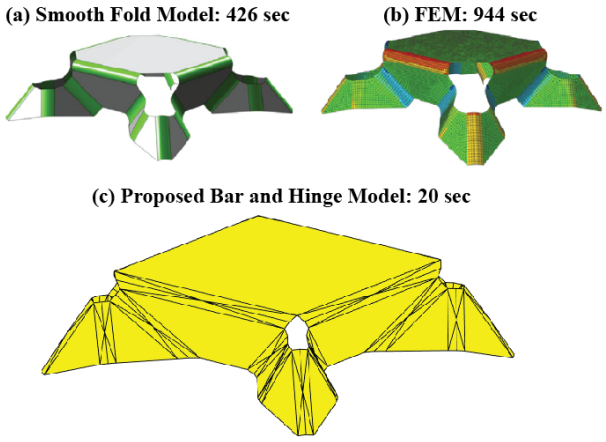

FIGURE 11. Folded shapes after loading of an origami pattern with compliant creases. (a) Smooth fold model; (b) FEM model; ((a) and (b) are images from [19]) (c) Simulation results of the proposed model.

shape for the origami (Fig. 11 (c)).

Simulation results and the computation time of the smooth fold model and FE simulation are obtained directly from [19]. The 20 second run-time for the bar and hinge model was recorded on a modern (2018) desktop computer with an i7-7700 processor. The proposed model was able to fold the structure with only about 5% of computation time needed for the smooth fold model. If only the global response and the geometry of the structure are of interest, using the proposed model can save a large amount of computational effort. However, the proposed model does not have a high resolution of the local response, so the smooth fold model or the FE simulation would be more suitable if the local response is of interest.

Bistable Miura Beam

In this section, the bistable behavior of a Miura-ori cantilever is studied. To demonstrate the bistable behavior, a physical paper model is made by gluing cardboard panels on a thinner printer paper. The panels are spaced evenly at 4.0 mm to create flexible compliant creases. By measuring the thickness of a stack of paper and then dividing by the total number of sheets, the thickness of printer paper is estimated to be 90 μm while the thickness of card board paper is estimated to be 500 μm. The Young's modulus of paper is assumed to be 2.0 GPa and the Poisson's ratio is assumed to be 0.3. The geometry of Miura pattern is defined in Fig.12 (a), and the parameters are set as: $a = b = 2.0$ cm; $\gamma = 80°$; $Extention = 0.998$. Two point loads with the same magnitudes but different directions are applied at the free end of the Miura beam (Fig.12 (b)). After the loading process, this paper model reached a second stable configuration as shown in Fig. 12 (c).

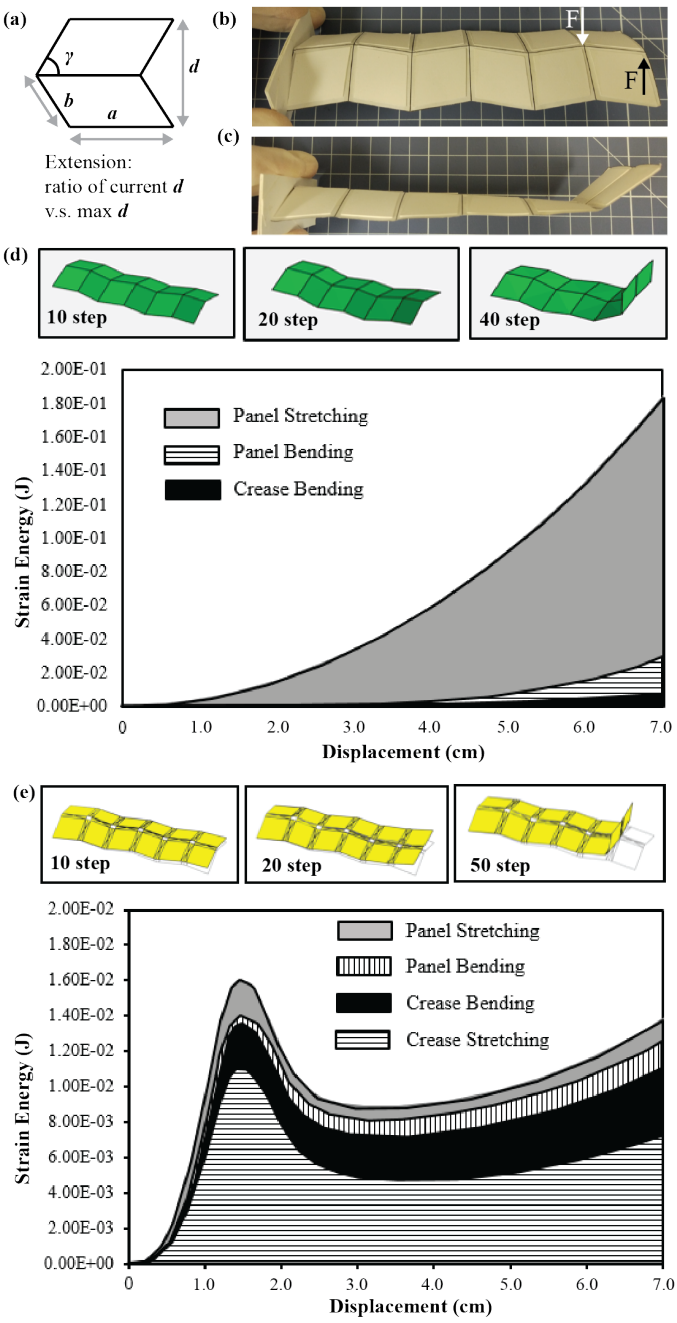

FIGURE 12. (a) Geometric definition of a Miura strip. $a = b = 2.0$ cm, *Extension* $= 0.998$, $\gamma = 80°$; (b) A physical paper model and loading set up; (c) The second stable configuration of this pattern; (d) Simulation results with the conventional bar and hinge model without compliant creases (MERLIN code); (e) Simulation results with the pro-posed bar and hinge model with compliant creases.

Both the proposed model with compliant creases and the conventional bar and hinge model were used to simulate this behavior. The publicly available MERLIN code [10] [25] was used as the representative of conventional bar and hinge models. Approximate calculations are used to convert the compliant crease properties so that they can be used to define stiffness in the conventional bar and hinge model. The crease bending stiffness K_f for a concentrated crease was calculated using the same pseudo-rigid crease model as Eqn. (8), and normalized by length using Eqn. (7). Using the geometry and assumed mechanical properties of paper, the crease bending stiffness is calculated as: $K_f = 0.03$ N $\cdot$ m/rad. Because the bending stiffness scales with the cubic of thickness, the panel bending stiffness of the conventional model was defined as: $K_b = (t_{panel}/t_{crease})^3 K_f = 170 K_f$. The bar areas were calculated using the same Eqn. (11) which results in $A_{bar} = 2.88 \times 10^{-6}$ m^2.

The simulated strain energy curves from the conventional model and the proposed model with compliant creases are shown in Fig. 12 (d) and (e) respectively. The two energy plots show that the proposed model can capture the second stable configuration of the origami (Fig. 12 (c)), which cannot otherwise be captured with a conventional model that ignores the geometry and extensional stiffness of compliant creases. Because the model with compliant creases has more degrees of freedom, it has an order of magnitude less strain energy for the same deformations as the conventional model. Additionally the local crease stretching energy dominates the total energy when the proposed compliant crease bar and hinge model is used. This behavior matches the "origami spring mechanism" (A cone like 4-vertex) proposed in [2]. During the bistable "pop through" of Miura beams, the extensional strain energy of creases contributes significantly to the energy barrier that creates the bistability. Such extensional stiffness of creases are neglected in the conventional bar and hinge models and thus, the bistable behavior of origami is not captured.

CONCLUDING REMARKS

This paper proposes an improved formulation for a bar and hinge model so that it can be used to study the behavior of origami assemblages with flexible compliant c reases. Equations for assigning bar areas and spring stiffness are derived by matching the stiffness of the bar and hinge model with a theoretical plate model. The proposed model is checked against FE simulations and the results match generally well under tensile, shear, bending, and torsional loading for infinitesimal deformation. The proposed model produces the best estimate of structural stiffness when the crease aspect ratio $\alpha \approx 0.1$ and the panel thickness ratio $\beta \approx 3.0$. These ratios are representative of real origami with compliant creases. At large deformations, the behavior of the proposed model is not sensitive to the α value and is able to give closely matched predictions when $\beta > 1.2$.

Examples were used to further demonstrate the capabili-

ties and efficiency of the model. In addition to capturing the crease bending for three dimensional folding simulations, the proposed model further captures the contribution from torsional and extensional behaviors of creases, which are of great significance when studying the bistable or multi-stable behaviors of origami inspired assemblages. The proposed model can be used as a fast and relatively accurate modeling technique for preliminary design of origami inspired assemblages with compliant creases, which provide the basis of various engineering structures or metamatrials with special mechanical properties.

ACKNOWLEDGMENT

The first author would like to acknowledge College of Engineering Dean's Fellowship and College of Engineering Challenge Fellowship from College of Engineering, University of Michigan. The authors also acknowledge support from DARPA Grant D18AP00071. The paper reflects the views and position of the authors, and not necessarily those of the funding entities.

REFERENCES

[1] Filipov, E. T., Tachi, T., and Paulino, G. H., 2015. "Origami tubes assembled into stiff yet reconfigurable structures and metamaterials". *Proceedings of National Academy of Science,* ***40***(112), pp. 12321–12326.

[2] Faber, J., Arrieta, A. F., and Studart, A. R., 2018. "Bioinspired spring origami". *Science,* ***359***, pp. 1386–1391.

[3] Yasuda, H., Tachi, T., Lee, M., and Yang, J., 2017. "Origami-based tunable truss structure for non-volatile mechanical memory operation". *Nature communications,* ***18***(962).

[4] Martinez, R. V., Fish, C. R., Chen, X., and Whitesides, M., 2012. "Elastomeric origami: Programmable paper-elastomer composites as pneumatic actuators". *Advanced Functional Materials,* ***22***, pp. 1376–1384.

[5] Lv, C., Krishnaraju, D., Konjevod, G., Yu, H., and Jiang, H., 2014. "Origami based mechanical metamaterials". *Scientific Report,* ***4***(5979).

[6] Fang, H., Chu, A., Xia, Y., and Wang, K. W., 2018. "Programmable self-locking origami mechanical metamaterials". *Advanced Materials,* ***30***(1706311).

[7] Tachi, T., 2009. "Simulation of rigid origami". In Origami 4, pp. 175–187.

[8] Tachi, T., 2009. "Generalization of rigid fodable quadrilateral mesh origami". In Proceedings of IASS.

[9] Filipov, E., Liu, K., Schenk, M., and Paulino, G., 2017. "Bar and hinge models for scalable analysis of origami". *International Journal of Solids and Structures,* ***124***, pp. 26–45.

[10] Liu, K., and Paulino, G., 2017. "Nonlinear mechanics of non-rigid origami: an efficient computational approach". *Proceedings of Royal Society A,* ***473***(20170348).

[11] Kawasaki, T., and Yoshida, M., 1988. "Crystallographic flat origamis". *Memoirs of the Faculty of Science, Kyushu University,* ***42***(2), pp. 153–157.

[12] Tachi, T., 2010. "Geometric considerations for the design of rigid origami structures". In Proceedings of IASS Symposium 2010.

[13] Wei, Z. Y., Guo, Z. V., Dudte, L., Liang, H. Y., and Mahadevan, L., 2013. "Geometric mechanics of periodic pleated origami". *Physical Review Letters,* ***110***(215501).

[14] Schenk, M., and Guest, S. D., 2013. "Geometry of miura-folded metamaterials". *PNAS,* ***110***(9), pp. 3276–3281.

[15] Liu, K., and Paulino, G., 2018. "Highly efficient structural analysis of origami assemblages using the MERLIN 2 software". In Origami 7.

[16] Bassik, N., Stern, G. M., and Gracias, D. H., 2009. "Microassembly based on hands free origami with bidirectional curvature". *Appl. Phys. Lett.,* ***95***(091901).

[17] Leong, T. G., Randall, C. L., Benson, B. R., Bassik, N., Stern, G. M., and Gracias, D. H., 2008. "Tetherless thermaobiochemically actuated microgrippers". *Proceedings of National Academy of Science,* ***106***(3), pp. 703–708.

[18] Yoon, C., Xiao, R., Park, J., Cha, J., Nguyen, T. D., and Gracias, D. H., 2014. "Functional stimuli responsive hydrogel devices by self-folding". *Smart Materials and Structures,* ***23***(094008).

[19] Hernandez, E. P., Hartl, D. J., Akleman, E., and Lagoudas, D. C., 2016. "Modeling and analysis of origami structures with smooth folds". *Computer-Aided Design,* ***78***, pp. 93–106.

[20] Hernandez, E. P., Hartl, D. J., and Lagoudas, D. C., 2017. "Kinematics of orgiami structures with smooth folds". In 25th AIAA/AHS Adaptive Structures Conference.

[21] Hernandez, E. P., Hartl, D. J., and Lagoudas, D. C., 2017. "Analysis and design of an active self-folding antenna". In ASME 2017 International Design Engineering Technical Conference and Computers and Information in Engineering Conference.

[22] Hur, D. Y., Hernandez, E. P., Galvan, E., Hartl, D., and Malak, R., 2017. "Design optimization of folding solar powered autonomous underwater vehicles using origami architecture". In ASME 2017 International Design Engineering Technical Conferences and Computers and Information in Engineering Conference.

[23] Howell, L., 2001. *Compliant Mechanisms*. John Wiley and Sons, Inc.

[24] Timoshenko, S. P., and Krieger, S. W., 1959. *Theory of plates and shells*. Mc Graw Hill Education. Page 5, Eqn(3).

[25] Liu, K., and Paulino, G., 2016. "Merlin: A matalab implementation to capture highly nonlinear behavior of non-rigid origami". In Proceedings of IASS Annual Symposium.